IMPROVED SHALLOW-WATER WAVE MODELING

Jane McKee Smith and Donald T. Resio

US Army Engineer Research and Development Center
Coastal and Hydraulics Laboratory
Vicksburg, Mississippi, USA

1.   INTRODUCTION

As coastal engineering projects become more complex, nearshore wave transformation models are required to provide more sophisticated results with greater efficiency. In the past, studies of nearshore sediment transport (shoreline change, channel shoaling, or response to engineering projects) required only the longshore variation of wave height and angle. Today, nearshore morphology change models require not only refraction, shoaling, and depth-limited breaking, but more advanced processes, including:

- Wave-current interaction
- Wind input
- Wave-wave interactions
- Whitecapping
- Wave-bottom interactions
- Diffraction
- Reflection
- Transmission
- Wave asymmetry

In addition to the requirement for more complex processes, nearshore transformation models must also meet the requirements of:

- Grid flexibility
- Efficiency
- Ease of application
- Robustness

Model efficiency is especially important as projects grow in scale (local to regional) and resolution. In the past, long time scales of wave transformation were calculated using a limited number of model runs covering the range of incident conditions. These results were stored in look-up tables, which were accessed to provide wave information over years of sediment transport calculation. Now, morphology models are sensitive to the interaction of waves, currents, and bed changes, thus requiring model applications to be closely coupled.

Finally, model users require extensive validation of wave transformation technology. Users need to understand model limitations and accuracy to provide the most effective model applications (whether they represent forecasts, hindcasts, or climate statistics for engineering design).

The nearshore wave model STWAVE has been a workhorse for the US Army Corps of Engineers and the coastal engineering community.   The model has evolved over the past 10 years to include wave-current interaction, improved breaking, and enhanced efficiency. Presently, an effort is ongoing to implement substantial improvements in STWAVE: full-plane transformation and generation, diffraction, reflection, bottom friction, and development of improved third-generation source terms. The impetus for this effort is failure of existing models in complex environments (e.g., tidal inlets, near structures) and failure of existing models to represent details of spectral evolution under both complex and simple wind forcing. Status of model upgrades is presented.

2.   HALF-PLANE VERSION OF STWAVE

The half-plane version of STWAVE, version 4.0 (Resio 1987, 1988; Smith, Sherlock, and Resio 2001; Smith and Smith 2002), was released 2001. This version of STWAVE includes refraction, shoaling, depth- and steepness-limited wave breaking, simplified diffraction, wave-current interaction, and second-generation wave growth (wind input, wave-wave interaction, and dissipation). The model simulates wave growth and transformation in a half plane (+/- 90 deg of the x axis). Advantages of the formulation are efficiency (including very small memory requirements), ease of application, and robustness. The input to the model includes no calibration or tuning parameters. Disadvantages include lack of flexibility (requires square grid cells), half-plane coverage (mean direction greater than 60 deg relative to the x axis lose significant energy), and lack of higher-order processes (diffraction, reflection, transmission, bottom interaction, and wave

asymmetry). The half-plane STWAVE have been validated through bench-marking studies (Ris et al. 2002, Smith 2000) and numerous project applications (e.g., Smith and Ebersole 2000, Smith and Smith 2001, and Smith and Gravens 2002,). The executable of STWAVE version 4.0 and support documentation is available on the CHL web site:

http://chl.erdc.usace.army.mil/CHL.aspx?p=s&a=Software;9

The half-plane version of STWAVE numerically solves the steady-state conservation of spectral action balance along backward-traced wave rays:

$$(C_{ga})_x \frac{\partial}{\partial x} \frac{C_a C_{ga} \cos(\mu - \alpha) E(f, \alpha)}{\omega_r} +$$

$$(C_{ga})_y \frac{\partial}{\partial y} \frac{C_a C_{ga} \cos(\mu - \alpha) E(f, \alpha)}{\omega_r} = \sum \frac{S}{\omega_r} \quad (1)$$

where

C_g = wave group celerity
x,y = spatial coordinates, subscripts indicate x and y components
C = wave celerity
μ = current direction
α = propagation direction of spectral component
E = spectral energy density
f = frequency of spectral component
ω = relative angular frequency
S = energy source/sink terms

and the subscripts a and r indicate absolute and relative quantities with reference to the current, respectively. Equation 1 is solved in two steps; first the energy is propagated (left-hand side of the equation) and then the source terms are applied (right-hand side of the equation). In the propagation step, wave rays for each frequency-direction bin of the spectrum are traced backwards one grid column to determine the point of origin, starting from the second column. The angle of the backtraced ray is determined by applying Snell's law, and then the spectral energy component is linearly interpolated between the closest grid points (the interpolation occurs in y direction) for each frequency–direction bin. The change in the width of the directional bins is also accounted for. Direction bins in the half-plane version are set to a constant 5 deg (with 35 total direction bins). Once the backtraced energy density is calculated, then Equation 1 is applied to determine the refracted and shoaled energy density at the grid point of interest. The entire grid column is transformed before source terms are applied. If currents are present and the wave-current interaction option is selected, the locally specified currents are used in the calculation of wave number and wave celerity in the refraction and shoaling calculations. STWAVE assumes a depth-averaged current and linear wave theory to calculate wave number, celerity, and group celerity.

STWAVE includes second-generation source terms. The source terms include wind input, nonlinear wave-wave interactions, high-frequency dissipation, and surf-zone breaking. Application of the first three source terms is optional, and the three are applied together to simulate wave generation from the wind. Wind speed and direction are specified as spatially constant across the model domain. For a wind speed to peak wave celerity greater than 0.98, downshifting of the spectral peak frequency is calculated as:

$$(f_p)_{i+1} = \left[(f_p)_i^{-3.33} + \frac{2.5 \Delta x}{g \cos(\alpha)} \left(\frac{u_*}{g} \right)^{1.33} \right]^{-0.3} \quad (2)$$

where f_p is the peak frequency, i is the grid column index, Δx is the grid spacing, g is gravitational acceleration, and u_* is the friction velocity. The energy added to the spectrum from the wind is given by:

$$F_{in} = \lambda \frac{\rho_a}{\rho_w} 0.85 C_p \frac{u_*}{g} \quad (3)$$

where λ is a partitioning coefficient (0.75), ρ_a is the density of air, ρ_w is the density of water, and C_p is the wave celerity associated with the spectral peak. Wave energy dissipation (white capping) is given by:

$$\Gamma_E = \frac{\varepsilon g^{\frac{1}{2}} E_{tot}^3 k_p^{\frac{9}{2}}}{\tanh^{\frac{3}{4}}(k_p h)} \quad (4)$$

where ε is a coefficient (=30), E_{tot} is the total energy, k is the wave number, the subscript p refers to the spectral peak, and h is local water depth. The dissipation is calculated independently for the spectral peak and for the low frequency range ($f < 0.6 f_p$) and summed. The angular distribution of input energy is $\cos^6$ and the frequency distribution relaxes to a TMA shape (Bouws et al. 1985) with a high-frequency tail of $k^{-2.5}$ (Resio et al. 2001).

The final source term, which is always applied, is the depth- and steepness-limited wave breaking:

$$H_{mo_{max}} = 0.1L \tanh kh \qquad (5)$$

where H_{mo} is zero-moment wave height and L is wavelength. This expression reduces to $H_{m0} = 0.63\,h$ in shallow water. Equation 5 is based on wave breaking in a strong ebb current (Smith, Resio, and Vincent 1997). This parametric formulation is applicable with or without currents.

STWAVE is a steady-state model (note the lack of a ∂/∂t term in Equation 1). For nearshore transformation, this is generally a good assumption if the wind and wave fields vary on a time scale greater than the wave propagation time across the grid and the spatial variation of the wind field is larger than the grid. Quasi-time varying runs are executed by simulating conditions every hour or several hours.

STWAVE has two offshore boundary conditions and two lateral boundary conditions. The default offshore boundary condition is a constant wave spectrum applied across the entire offshore boundary ($x = 0$). There is also an option that allows multiple spectra to be specified on the offshore boundary. STWAVE interpolates these spectra onto the offshore grid points using either linear or morphic interpolation. If wave directions vary by 10-15 deg or more between the input spectra, linear interpolation can cause smearing or splitting of the directional distribution. The morphic method was developed to preserve the general form of the directional distribution (Smith and Smith 2002). Nesting options in STWAVE automate the process of nesting and interpolating spectra between coarse- and fine-grid applications. Lateral boundary conditions in STWAVE can be specified as either closed or open. Closed boundaries are specified by placing land points on the lateral boundary, which allows no energy to enter along the boundary. Placing water points on the boundary specifies open boundaries. On open boundaries, wave propagation is calculated by reflecting interior grid points across the boundary to provide the origin of the back-traced rays. This method assumes approximate plane and parallel contours along the lateral boundaries and minimizes boundary effects in the grid interior.

The inputs required to execute STWAVE are as follows:

- Bathymetry grid (including shoreline position, grid size, and grid resolution).

- Incident frequency-direction wave spectrum on the offshore grid boundary.
- Current field (optional).
- Tide elevation, wind speed, and wind direction (optional).

STWAVE output includes the following

- Wave height, peak period, and mean direction over the entire grid.
- Wave spectra and parameters at specified locations.
- Radiation stresses over the entire grid for input to circulation models (optional).
- Indices indicating regions of wave breaking (or breaking-induced dissipation) over the entire grid.

STWAVE is included in the Surface-Water Modeling System Graphical User Interface (Brigham Young University Engineering Computer Graphics Laboratory 1997). The interface can be used to generate bathymetry grids, input spectra, and the model options file. The interface also provides visualization capabilities, including contour plots of wave height, period, and direction; vector plots of wave and current direction; and plots of one or two-dimensional spectra.

3. FULL-PLANE VERSION OF STWAVE

The full-plane version of STWAVE is not a replacement for the half-plane version, but a supplement. The versions will eventually be combined into a seamless application. The half-plane version will always have an advantage of substantially lower memory requirements (~ two orders of magnitude) and faster execution. The half-plane limitation is generally appropriate for nearshore coastal applications, with the exception of enclosed or semi-enclosed bays, estuaries, and lakes where seas and swells may oppose each other or there is no clear "offshore" direction. The full-plane version allows wave input on all boundaries and wave generation from all directions.

The full-plane version of STWAVE is based on Equations 1-5, like the half-plane version. Propagation is solved in four sweeps. Each sweep covers a quadrant of the grid (i.e., 0-90 deg, 90-180 deg, 180-270 deg, and 270-360 deg, relative the to grid x axis). The order of the sweeps is dependent on the wind direction. The half-plane opposite the wind direction is solved first, and then the half-plane coincident with the wind direction. The propagation is solved by alternating sweep directions in each half plane for propagation. Wave generation is calculated immediately following

the final propagation sweep for each cell. Thus, similar to the half-plane version, generation is calculated following propagation. The alternating method reduces the number of iterations required for the entire grid. Presently, the number of iterations is set by the user. For relatively simple bathymetry, generally only one or two iterations are necessary. For complex bathymetries, where wave direction varies significantly across the grid, multiple iterations may be required. A single iteration of the full-plane version is approximately 4.5 times slower than the half-plane version. The full-plane version has not yet been optimized.

Within the full-plane version, growth of a new wave train is initiated if the mean wave and wind directions differ by more than 90 deg. For differences less than 90 deg, the wind will grow and turn the propagated wave field. Sea and swell components are tracked separately in the model.

The full-plane version provides some additional improvements to the model:

- Grid cells are rectangular, so x and y grid spacing is not required to be the same. Also, the directional resolution is no longer limited to 5 deg, but is specified by the user.
- A spectral generator is now included in the code, so TMA-shaped input spectra can be generated with input of wave height, peak period, and mean direction.
- Planar bathymetry grids can also be generated within the model for simple applications.
- Wave number is computed prior to propagation to avoid redundant calculations. These values are used for all sweeps and interactions, and they are carried through to additional input conditions, if tide and current do not change. This reduces computational burden, but increases memory requirements.

The full-plane version does not presently have a lateral boundary condition equivalent to the 'open' lateral boundary in the half-plane version. This is because wave input can now be specified on all boundaries of the grid, and thus, there are no default lateral sides to the grid. A lateral boundary condition will be added assuming one-dimensional propagation along a specified boundary. Presently, lateral boundaries must be set away from the area of interest, so their impact is minimized.

A range of benchmark cases have been simulated with the full-plane version. One of these cases is Grays Harbor, Washington, USA. Grays Harbor includes a complex ebb shoal and an inlet channel. For this case, STWAVE converged by approximately an order of magnitude with each iteration. For example, the mean change in wave height between the first and second iteration was 3.4×10^{-3} m, second and third was 2.6×10^{-4} m, and third and fourth was 1.9×10^{-5} m. The mean direction convergence was an order of magnitude or greater: 3 deg, 0.025 deg, and 0.005 deg, for second, third, and fourth iterations, respectively. Figure 1 shows comparisons of the half-plane and full-plane version for Grays Harbor, Washington. The incident wave conditions for this case were wave height of 4.3 m, peak period of 11 sec, and mean direction of 256 deg. The difference is calculated as the full-plane height minus the half-plane height. Wave periods were approximately constant. The results in the offshore are identical, but there are differences in the inlet entrance, near structure, shorelines, and channels, where wave directions become oblique to the half-plane grid. The differences arise from the limitation of all energy propagating from the previous grid column in the half-plane version. Both versions of the model were run with closed lateral boundaries.
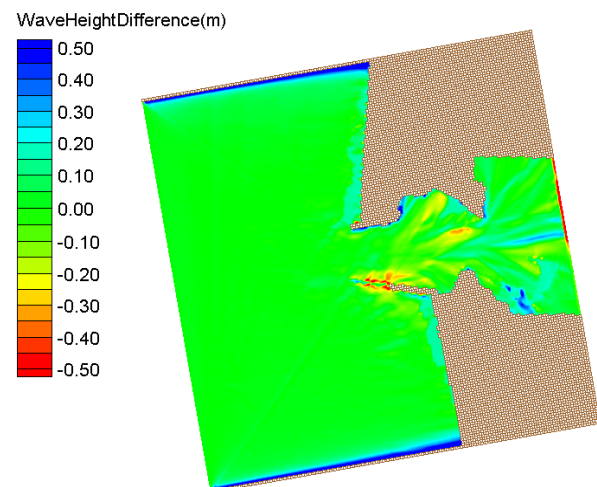

Figure 1. Example wave height differences between full- and half-plane versions STWAVE for Gray Harbor, Washington (25 Sep 1999, 0400), brown indicates land.

4. ON-GOING MODEL IMPROVEMENTS

A number of additional model improvements are in progress. The goal is to develop an accurate and efficient model for application in a range of complex environments. Planned improvements include: bottom interaction, diffraction and reflection, and third-

generation source terms.

4.1 Bottom Interactions

Bottom friction and wave-mud interactions have not been included in standard versions of STWAVE because of the lack of validation data and general guidance in their application. Data are now becoming available (e.g., Sheremet and Stone 2003) to quantify and validate wave-bed interactions. These interactions may prove to be critical for accurate modeling of areas with very shallow shelves, reefs, or mud bottoms.

4.2 Diffraction and Reflection

Holthuisen et al. (2003) have shown that even in situations with complex bathymetry, diffraction in most wave spectra can be modeled via a phase-averaged diffusion operator; however, these authors point out that such an approximation may not be very good in the vicinity of a hard, surface-piercing structure. Mase (2001) derives a mathematical representation of the diffraction process that works very well for relatively broad spectra even near structures; however, the accuracy of this representation diminishes for spectra with very narrow directional spreads. As part of an ongoing effort to update STWAVE, a new method for representing diffraction in spectral models has been formulated. This form preserves solution accuracy in both the near field and far field of the domain, even for the case of very narrow spectra near structures.

A single spectral component (or its monochromatic counterpart) will have a velocity potential of the form

$$\phi = \frac{g}{\omega} \frac{\cosh[k(h+z)]}{\cosh(kh)} a e^{-i\omega t} \qquad (6)$$

where z is the vertical coordinate with zero at the water surface, a is the topography of the free surface at time = 0 (basically an amplitude function in x and y), and t is time. Since the velocity potential is irrotational, we must have

$$\frac{\partial^2 a}{\partial x^2} + \frac{\partial^2 a}{\partial y^2} + k^2 a = 0 \qquad (7)$$

If we consider a second function such that

$$\varphi = \frac{\cosh[k(h+z)]}{\cosh(kh)} D_0(kr) e^{-i\omega t} \qquad (8)$$

it can be shown that φ also satisfies the Laplace equation, and we have

$$\frac{\partial^2 D_0}{\partial x^2} + \frac{\partial^2 D_0}{\partial y^2} + k^2 D_0 = 0 \qquad (9)$$

Using Green's theorem and noting that the form of D_0 can be written in terms of Bessel functions of order zero, the complex amplitude of a wave inside a bounded region can be written as an integral around the boundary (similar to the derivation of wave diffraction in the Huyghens-Kirchoff integral used in optics),

$$a_p = \oiint_S \frac{a(s)}{\sqrt{r}} \frac{\cos(\theta) + \cos(\alpha)}{2} e^{-i(\rho_0(s) + kr - \pi/4)} ds \qquad (10)$$

where a (s) is the amplitude at point "s" along the boundary S, ρ_0 (s) is the phase of the complex amplitude at s, r is the distance from the boundary to point "p", θ is the direction from "s" to "p", and α is the wave propagation angle at "s." For the case of a straight-line boundary (ignoring 180^0 reflections) and normalizing r by the wavelength, this can be written as

$$a_p = \int_Y \frac{a(y)}{\sqrt{y}} \frac{\cos(\theta) + \cos(\alpha)}{2} e^{-i[2\pi(y\sin\alpha + r) - \pi/4]} dy \qquad (11)$$

where the integral proceeds along y over the line segment "Y." This form for diffraction allows for a variation in wave height along Y rather than requiring a constant wave height as in a Fresnel integral form for diffraction but is otherwise quite similar to that representation, with the added stipulation that a near-field solution form can be used in the representation shown here in place of the $\sqrt{r}$ denominator.

Berkoff (1973) showed that the combined effects of refraction and diffraction could be solved via the "mild-slope approximation"

$$\frac{1}{a}\left\{\Delta a + \frac{1}{cc_g}\nabla a \cdot \nabla(cc_g)\right\} + k^2 - \nabla\rho \cdot \nabla\rho = 0 \qquad (12)$$

and

$$\nabla \cdot (a^2 cc_g \nabla\rho) = 0 \qquad (13)$$

where c is the wave phase velocity c_g is the wave group velocity, and ρ is wave phase along the ray. The first equation is the eikonal equation for the refracted-diffracted ray and the second is the condition for energy conservation along the ray. The second term within the curly brackets is the combined refraction-diffraction

coupling term. Accurate solution of this equation requires a resolution in x and y such that the grid increment is smaller than L/8.

A singularity in the amplitude function exists at the boundary of a surface-piercing structure. The sharp interference patterns in monochromatic waves passing by such a structure are created by the superposition of the diffracted wave from this singularity and the geometric wave passing by it. Near a singularity, we have

$$
\frac{\frac{\partial a}{\partial y}}{\frac{\partial^2 a}{\partial y^2}} \to 0 \tag{14}
$$

as $y \to 0$. This suggests that the diffraction pattern will depend primarily on the first term in the curly brackets near a structure, with a secondary (relatively slow) dependence on refraction and other processes. In such cases, it is possible to adapt a series solution for this problem, i.e.

$$
\vec{\Gamma}_p = \vec{\Gamma}_p^{(0)} + \vec{\Gamma}_p^{(1)} + \cdots \tag{15}
$$

where $\vec{\Gamma}_p$ is the energy flux vector at "p" and the superscripts "(0)" and "(1)" refer to the order of magnitude of the terms. In this case, we allow the diffraction solution to represent order zero and add the effects of refraction as a second step to the solution.

The solution for diffraction is very accurate provided that the resolution along y is sufficiently small, say on the order of L/20. However, its solution is quite slow numerically on such a scale; hence direct solution of the Huyghens-Kirchoff form for diffraction is too cumbersome for most wave modeling purposes. Thus, instead of the exact form, we substitue a pre-solved, discretized complex operator D, defined as

$$
\{R[D(\delta y, \delta x, \alpha), I(\delta y, \delta x, \alpha)]\} \tag{16}
$$

where R is the real part of the H-K integral and I is the imaginary part of the H-K integral for an incident wave of unit amplitude. The terms inside the parentheses denote the resolution in y and x for fixed values of α, respectively. After sensitivity testing, these have been set in the current version of the code to $\delta y = L/400$, and $\delta x = L/10$. Inside STWAVE diffraction then becomes represented as a simple inner product with amplitude

$$
| a_p | = [\sum_{k=1}^{M} a_k R_k (\delta x, \delta y, \alpha)]^2 +
$$
$$
[\sum_{k=1}^{M} a_k I_k (\delta x, \delta y, \alpha)]^2 + R_B + I_B \tag{17}
$$

where M is taken to cover a sufficient range in y to provide an accurate approximation to the total integral. R_B and I_B in this equation represents real and imaginary boundary integrals taken to infinity, effectively taking the phase, rate of phase variation along y, and the amplitude of the last point and treating it as though this wave extended to infinity. This step was added to eliminate diffraction from boundary discontinuities.

The phase of the wave at "p" is given by

$$
\rho_p = \tan^{-1}\left(\frac{\Sigma_I}{\Sigma_R}\right) \tag{18}
$$

where Σ_I and Σ_R are the sum of the imaginary and real contributions to the H-K integral, respectively. The energy flux angle at "p" is found from

$$
\alpha_\Gamma = \sin^{-1}\left(\frac{k \partial \rho_p}{\partial y}\right) \tag{19}
$$

By shifting the discretized elements of the operator $\pm n$ positions along y, a simple estimate of the angle can be obtained that is not directly dependent on the scale of the grid resolution.

Treating the diffraction-only solution in terms of a field equation for the rays, we can represent the effects of refraction on path (flux angle and displacement) and amplitude as

$$
y_I^{(1)} = y^{(0)} + \sum_{i=I_0+1}^{I} \delta y_i (x, y)^{(0)}
$$
$$
\alpha_I^{(1)} = \alpha^{(0)} + \sum_{i=I_0+1}^{I} \delta\alpha_i (x, y)^{(0)} \tag{20}
$$
$$
a_I^{(1)} = a^{(0)} \prod_{i=I_0+1}^{I} S_{r_i} (x, y)^{(0)}
$$

where I_0 references the x-location of the boundary and I references the location of the point at "p." The term S_{r_i} references the effective change in amplitude along the ray due to refraction at the Ith column of the grid.

To implement additional source terms such as wave breaking, this is modified to the form

$$a_I^{(2)} = a^{(0)}(x_0, y_0) \prod_{i=I_0+1} S_{r_i}(x, y) S_{e_i}[a^{(1)}(x, y)^{(1)}] \quad (21)$$

where the term S_{e_i} represents the sum of all additional source terms considered at the Ith column of the grid.

Figures 2 and 3 show the modeled results for the amplitude and angle, respectively, of a monochromatic wave propagating perpendicular to a single "one-arm" breakwater. The incident wave height is 0.62m, the period is 10 sec, and the direction is normal to the breakwater. The water depth at the breakwater is 15 m, and the bathymetry behind the breakwater slopes up to 1 m and then back to 15 m. The plots are given for a distance of 0.7 L behind the breakwater. The breakwater shadow zone is grid cells 1 to 10 ($\Delta x = 15.7$ m). In these figures the red line represents the solution with no refraction, shoaling, and breaking, while the green line represents the solutions with those effects added. The solution is an excellent approximation to the exact integral solution for this case. The differences in the solutions in wave height are due to breaking over the shallow bathymetry, and the differences in wave direction in the shadow zone are due to refraction. Figures 4 and 5 show results for waves propagating through a breakwater with two gaps. The incident wave conditions, bathymetry, and grid resolution are the same as the one-arm breakwater case. The breakwater shadow zones are cells 1-10, 19-23, and 32-41. Note the symmetry in wave height and direction around the center of the middle breakwater.
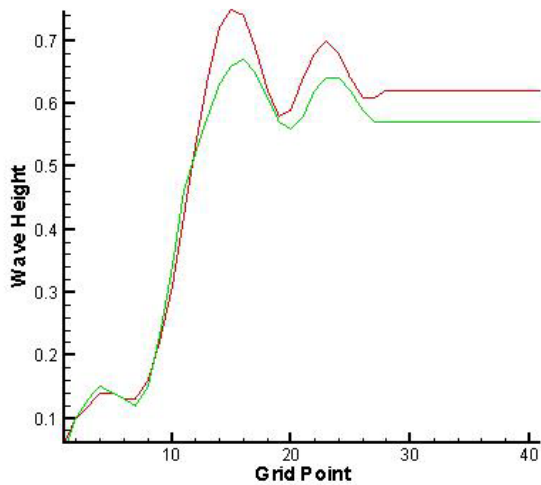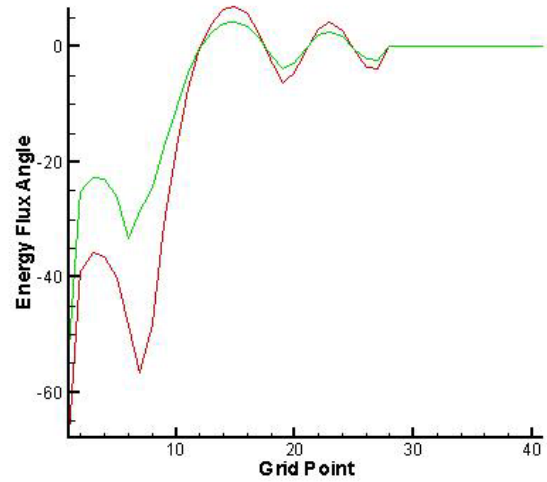

Figure 3. Wave angle (deg) behind a one-arm breakwater (red is diffraction only, green is with refraction, shoaling, and breaking).
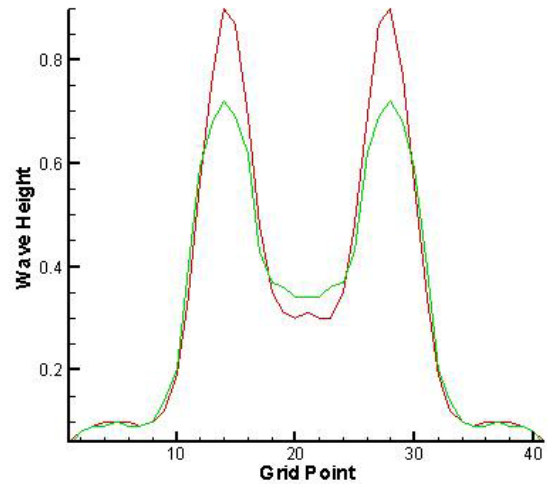

Figure 4. Wave height (m) behind a breakwater with two gaps (red is diffraction only, green is with refraction, shoaling, and breaking).

Figure 2. Wave height (m) behind a one-arm breakwater (red is diffraction only, green is with refraction, shoaling, and breaking).
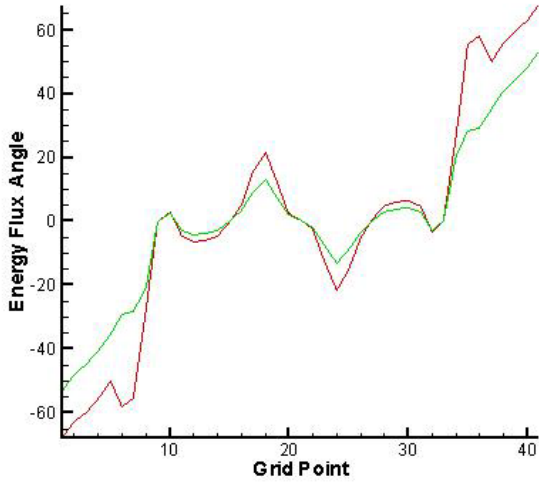
Figure 5. Wave angle behind a breakwater with two gaps (red is diffraction only, green is with refraction, shoaling, and breaking).

Single and/or multiple reflections can be represented in terms of a geometric expansion of the form

$$a_p = \sum_{k=1}^{N} \int_{aperture} \frac{\beta^{k-1} a(y)}{r} \frac{\cos\alpha_{k-1} + \cos\theta}{2} e^{-i\rho'} dy \quad (22)$$

where

$$\alpha_0 = \alpha$$
$$\alpha_k = -\alpha_{k-1}$$

where N is the number of apertures required to cover a sufficient integration domain, β is the reflection coefficient, and k is the number of reflections encountered enroute to "p." Figure 6 shows the results for a unidirectional, monochromatic wave propagating along a completely absorbing wall (β=0). The incident wave conditions are the same as the previous example ($H = 0.62$m, $T = 10$ sec, and the wave direction is parallel to the wall. The wall is located at grid point 10. As expected, this solution is equivalent to the case of a "one-arm" breakwater. Figure 7 shows the results for a wave propagating along a completely reflective wall (β=1) for the same incident wave condition. The simulation exactly preserves the wave height across the domain, which is expected since this situation mimics the case of non-absorptive waveguides.
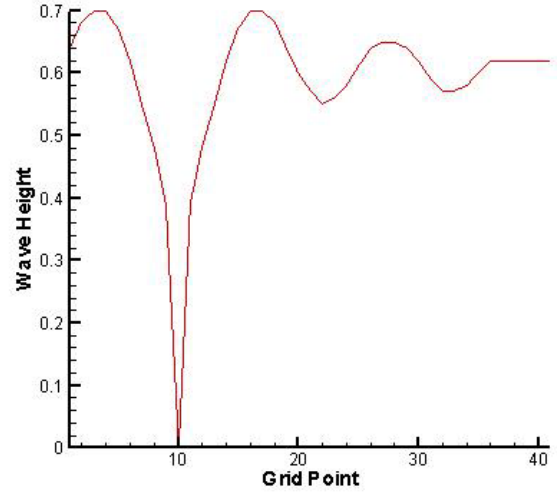

Figure 6. Wave height (m) along a fully absorbing wall (wall is at grid point 10).
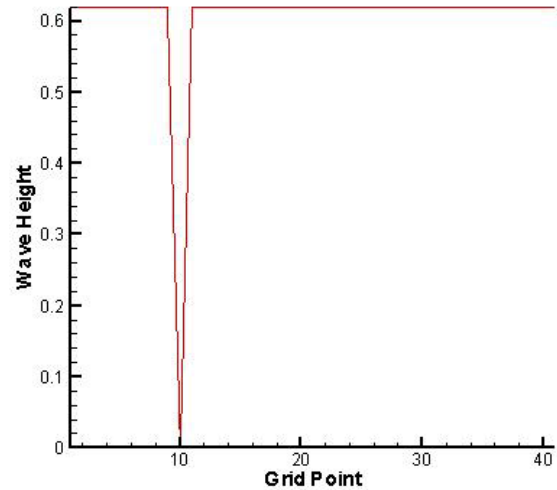

Figure 7. Wave height (m) along a fully reflecting wall (wall is at grid point 10).

4.3 Third-Generation Source Terms

As described in Resio *et al.* (2004), source terms in existing third-generation wave models are not considered adequate for coastal applications. The first major problem is that the Discrete Interaction Approximation (DIA), used for estimating the wave-wave interaction source term in such models, does not provide a good representation of complex spectra typical of coastal areas as shown in Figure 8. A second major problem is that the shallow-water form for wave-wave interactions used in such models is based on the

work of Heterich and Hasselmann (1980). As was pointed out by Heterich and Hasselmann, this approximation very strictly limited to applications in which $k_p h \geq 1$. Such a situation is reached in moderate rather than shallow water for most ocean waves, e.g., a 10-sec wave period in 20 m water depth. Resio *et al.* (2004) show that the source–term approximation based on the Heterich and Hasselmann (1980) scaling is highly inaccurate past this limit (Figure 9) and is not appropriate for shallow coastal areas.

Scaled source term for T_p 12 sec. JONSWAP spectrum in 10 meters Compared to actual computed values. ($k_p h = 0.55$)

Scaled S_{nl}

Actual S_{nl}

But models such as SWAN are often applied for kh values that are much smaller than this!

Figure 9. Example comparison of wave-wave interactions (S_{nl}) for exact solution (green line) and Heterich and Hasselmann scaling (red line).
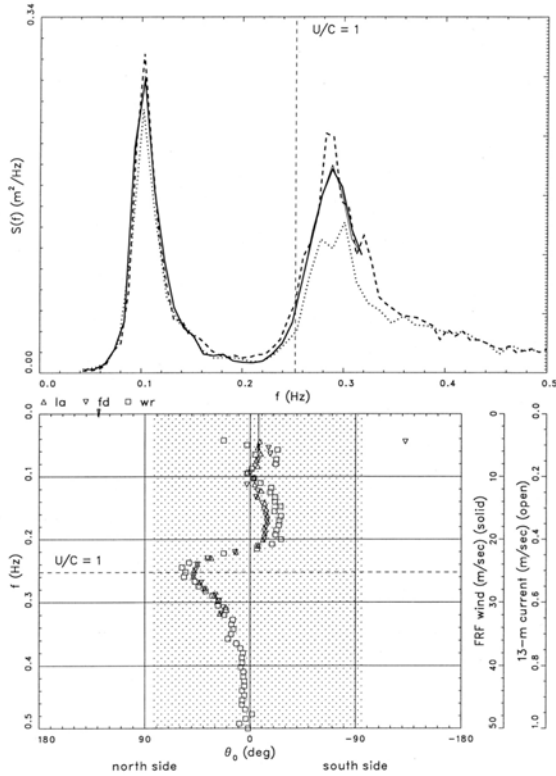

Figure 8. Measured coastal wave frequency spectra and mean direction by frequency from the Field Research Facility, Duck, NC. Dashed line is in 16.6 m depth, solid line is 7.7 m depth, and dotted line is 8.1 m depth.
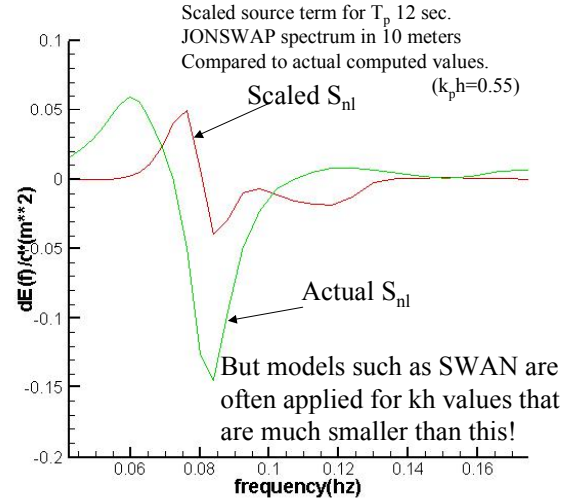
5. SUMMARY

Sophisticated coastal processes studies require accurate, efficient, and flexible nearshore wave transformation models. These applications also demand more advanced wave processes. A major effort in now underway to reformulate appropriate source terms for third-generation wave models in coastal areas. These are expected to be completed within the next year and include:

- new wind input function,
- new wave breaking function,
- new arbitrary-depth representation for wave-wave interactions, and
- incorporation of three-wave interactions based on a kinetic equation approach.

These new source terms will replace the existing second-generation source terms as work is completed and results in the new version of STWAVE are validated. Work is also ongoing to incorporate diffraction, reflection, and bottom interaction Bench marking of model capabilities will remain a priority. As model physics are improved, more robust applications of wave models can be made without tuning coefficients or formulations to each application.

6. ACKNOWLEDGEMENTS

Transformation-Scales Waves work unit in the Navigation Systems Program of the Coastal and Hydraulics Laboratory, U.S. Army Engineer Research and Development Center.

7. REFERENCES

Berkhoff, J. C. W., 1972: Computation of combined refraction-diffraction. *Proc.,* 13th International Conference on Coastal Engineering, ASCE, 471-490.

Bouws, E., Gunther, H., Rosenthal, W., and Vincent, C. L., 1985: Similarity of the wind wave spectrum in finite depth waves; 1. Spectral form. *Journal of Geophysical Research*, 90(C1), 975-986.

Brigham Young University Engineering Computer Graphics Laboratory, 1997: Surface-water modeling system reference manual. Brigham Young University, Provo, UT.
http://hlnet.wes.army.mil/software/sms/docs.htp

Herterich, K., and Hasselmann, K., 1980: A similarity relation for the nonlinear energy transfer in a finite-depth gravity-wave spectrum. J. Fluid. Mech., Vol. 97, 215-224.

Holthuijsen, L. H., et al., 2003: SWAN user manual: SWAN cycle III version 40.20. Delft, Netherlands, Faculty of Civil Engineering and Geosciences, Environmental Fluid Mechanics Section, Delft University of Technology, 128.

Mase, H., 2001:   Multi-directional random wave transformation model based on energy balance equation. *Coastal Engineering Journal*, 43(4), JSCE, 317-337.

Resio, D. T., 1987: Shallow-water waves. I: Theory. *Journal of Waterway, Port, Coastal, and Ocean Engineering*, 113(3), ASCE, 264-281.

Resio, D. T., 1988: Shallow-water waves. II: Data comparisons. *Journal of Waterway, Port, Coastal, and Ocean Engineering*, 114(1), ASCE, 50-65.

Resio, D. T., Pihl, J. H., Tracy, B. A., and Vincent, C. L. 2001: Nonlinear energy fluxes and the finite depth equilibrium range in wave spectra. *J. Geophys. Res*., 106(C4), 6985-7000.

Resio, D.T., Long, C.E., and Perrie, W., 2004: The dynamics of spectral equilbria: Part 1 Detailed-balance physics, 8th International Workshop on Wave Hindcasting and Forecasting, Turtle Bay, Hawaii.

Ris, R., Holthuijsen, L., Smith, J.M., Booij, N., and van Dongeren, A., 2002: The ONR test bed for coastal and oceanic wave models. *Proceedings*, ICCE 2002, World Scientific, 380-391.

Sheremet, A., and Stone, G.W., 2003: Observations of nearshore wave dissipation over muddy sea beds. *J. Geophys. Res*., 108(C11), 21-1-11.

Smith, J. M., 2000: Benchmark tests of STWAVE. *Proceedings*, 6th International Workshop on Wave Hindcasting and Forecasting, Environment Canada, 169-379.

Smith, J. M., and Ebersole, B. A., 2000: Modeling and analysis of short waves. Chapter 5 in Study of navigation channel feasibility, Willapa Bay, Washington. Technical Report ERDC/CHL-00-6, N. C. Kraus, ed., U.S. Army Engineer Research and Development Center, Vicksburg, MS, 23 pp.

Smith, J. M., and Gravens, M.B., 2002: Incident boundary conditions for wave transformation. *Proceedings*, 7th International Workshop on Wave Hindcasting and Forecasting, Environment Canada, 373-384.

Smith, J. M., Resio, D. T., and Vincent, C.L., 1997: Current-induced breaking at an idealized inlet. *Proceedings*, Coastal Dynamics '97, ASCE, 993-1002.

Smith, J. M., Sherlock, A. R., and Resio, D. T., 2001: STWAVE: steady-state spectral wave model; user's manual for STWAVE Version 3.0. Instruction Report, U.S. Army Engineer Research and Development Center, Vicksburg, MS.

Smith, J. M., and Smith, S. J., 2002: Grid Nesting with STWAVE.   Coastal and Hydraulics Engineering Technical Note CHETN I-66, U.S. Army Engineer Research and Development Center, Vicksburg, MS. *http://chl.wes.army.mil/library/publications/chetn/*

Smith, S. J., and Smith, J. M., 2001: Numerical modeling of waves at Ponce de Leon Inlet, Florida. *J. Waterway, Port, Coastal and Ocean Engineering*, 127(3), 176-184.